Energy & Environmental Science

www.rsc.org/ees

Volume 6 | Number 10 | October 2013 | Pages 2779–3100

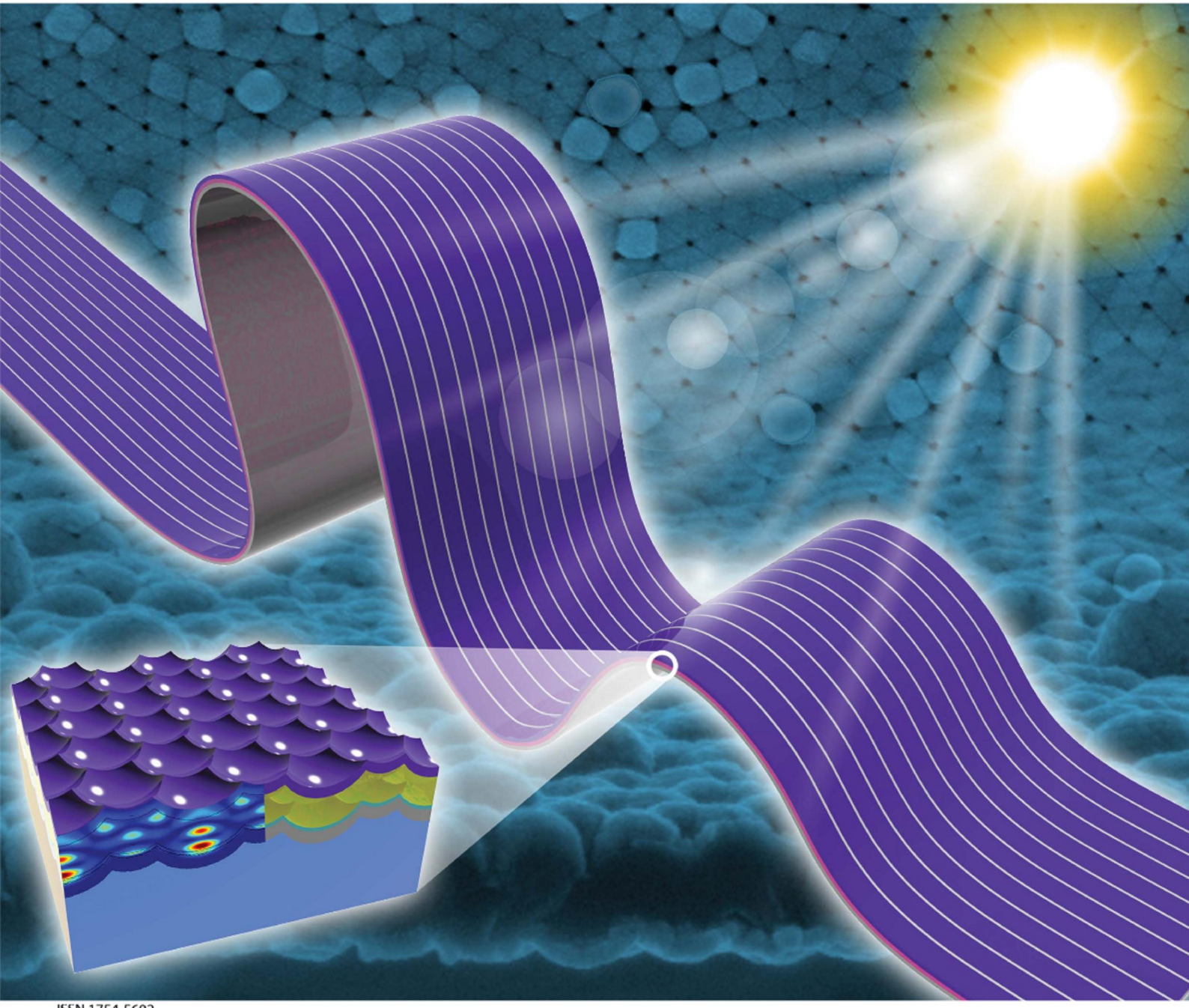

ISSN 1754-5692

RSC Publishing

PAPER

Shen, Li, Fan *et al.*

Performance enhancement of thin-film amorphous silicon solar cells with low cost nanodent plasmonic substrates

Energy & Environmental Science

RSC Publishing

PAPER

Performance enhancement of thin-film amorphous silicon solar cells with low cost nanodent plasmonic substrates†

Cite this: *Energy Environ. Sci.*, 2013, **6**, 2965

Hongtao Huang,[ab] Linfeng Lu,[b] Jun Wang,[b] Jie Yang,[b] Siu-Fung Leung,[c] Yongqian Wang,[d] Di Chen,[a] Xiaoyuan Chen,[b] Guozhen Shen,‡*[a] Dongdong Li*[b] and Zhiyong Fan*[c]

Received 3rd April 2013
Accepted 5th June 2013

DOI: 10.1039/c3ee41139g

www.rsc.org/ees

Performance of thin film photovoltaics largely relies on photon absorption capability. Here, we introduce a novel substrate with patterned aluminum nanodent arrays with unique light management capability. Hydrogenated amorphous silicon thin film solar cells have been fabricated on the nano-texturized substrate for optical property study and photovoltaic performance evaluation. Our measurements have shown significant enhancement on broadband light absorption using these patterned substrates *via* both geometrical light trapping and plasmonic coupling. Particularly, the enhancement factor reaches as high as 5–30 times at wavelength near the band edge. Numerical simulations confirm the measurements and uncover the mechanisms of the enhancement. More importantly, photovoltaic measurements on nanodent solar cells present improvements of over 31% and 27% in short circuit current and energy conversion efficiency respectively compared with planar solar cells. Therefore, the novel patterned substrates are promising candidates for low cost and high performance thin film solar cells.

Broader context

Among various alternative energy sources, solar power is of great advantage over other candidates due to its abundance and environmental friendliness. Current solar cells still cannot satisfy people's expectation on performance and cost. Aiming at promoting the ability of harvesting solar power as well as reducing the manufacturing cost, a novel plasmonic substrate was developed using a convenient anodization method for thin film amorphous silicon solar cells, which convert solar power into electricity within a very thin absorbing layer. According to experimental and finite-difference time-domain simulations, the devices exhibit impressive light trapping capability, due to the coupling of waveguide modes and surface plasmon resonances with the aid of nanoscale patterns. The optimized device configuration delivered 5–30 times absorption enhancement near the band edge. The optical absorption and propagation were systematically investigated in view of photonic guided modes and surface plasmon resonances as well as their coupling effects. In comparison to the device on planar substrates, the plasmonic solar cells achieved significantly increased short circuit current (31%) with a promising energy conversion efficiency up to 7.11%.

1 Introduction

Hydrogenated amorphous silicon (a-Si:H) thin-film solar cells are promising candidates for large scale deployment of photovoltaics, owing to their advantages of low cost, material abundance, non-toxicity, mature processing technology and compatibility with various types of substrates. However, these advantages are offset by poor crystallinity and existence of dangling bonds in a-Si:H resulting in short carrier diffusion length and instability upon prolonged illumination.[1] It is known that using thinner absorbing layers leads to reduced impact of the Staebler–Wronski (S–W) degradation, improved effective carrier separation and collection, and higher open circuit voltage.[2] However, the dilemma is that the incident light, especially in the spectral range near band edge, cannot be absorbed sufficiently within such thinner absorbing layers. Therefore, developing high efficiency solar cells involves the trade-off between the optimal electrical and optical performances.

Besides the conventionally utilized surface textures, such as textured TCO glass[3,4] or chemical etched pyramid arrays on silicon wafers,[5] new techniques have been employed based on nanomaterials to improve optical absorption of solar cells. One dimensional nanostructure arrays, such as nanopillars,[6,7]

[a]*Wuhan National Laboratory for Optoelectronics and College of Optoelectronic Science and Engineering, Huazhong University of Science and Technology, Wuhan, 430074, China. E-mail: gzshen@hust.edu.cn*

[b]*Shanghai Advanced Research Institute, Chinese Academy of Sciences, 99 Haike Road, Zhangjiang Hi-Tech Park, Pudong, Shanghai 201210, China. E-mail: lidd@sari.ac.cn*

[c]*Department of Electronic and Computer Engineering, Hong Kong University of Science and Technology, Clear Water Bay, Kowloon, Hong Kong, China. E-mail: eezfan@ust.hk*

[d]*Suntech Power Holdings Co., Ltd., 9 Xinhua Road, New District, Wuxi, Jiangsu Province 214028, China*

† Electronic supplementary information (ESI) available. See DOI: 10.1039/c3ee41139g

‡ Current address: State Key Laboratory for Superlattices and Microstructures, Institute of Semiconductors, Chinese Academy of Sciences, Beijing 100083, China.

nanospikes,[8] nanowires[9] and nanoholes,[10,11] have demonstrated improved anti-reflection and extended broadband absorption, mainly due to a gradient in effective refractive index from the top of the structure to the bulk material and increased optical path length induced by scattering.[12] In addition to structural light trapping, recently, plasmonic nanostructures have been introduced into solar powered devices with different configurations showing remarkable optical absorption enhancement.[13–22] Typically, metal nanostructures were embedded at the front or rear side of solar cells.[14,23–25] Surface plasmon resonances of these nanostructures result in enhanced light scattering and increased optical path length within the absorbing layer. For example, a 23% enhancement in energy conversion efficiency has been presented on solar cells incorporated with 200 nm nucleated silver nanoparticles.[26] On substrates composed of nanopillar, nanodome and nanocone arrays, plasmonic back reflectors have also been utilized to improve the optical performance of a-Si:H solar cells, among which solar cells on nanocone array substrates presented the highest efficiency (10.9%) owing to the absence of structural defects at the sharp corners on the nanostructured substrates.[27–29]

Implementation of the aforementioned light management schemes largely relies on costly nanofabrication with limited scalability; however, the cost-effectiveness is crucial for a thin film photovoltaic technology. In this work, we demonstrate a simple route towards patterned plasmonic silver back reflectors on aluminum foil for enhanced optical absorption of a-Si:H solar cells and reveal the improvement mechanisms by finite difference time domain (FDTD) simulations. Large-scale quasi-ordered nanodent arrays are obtained on Al foils and conformal Ag films are used as the back reflectors by direct current sputtering. The wavelength scale nanodent arrays serve as scattering textures and contribute to the excitation of waveguide modes in a-Si:H and surface plasmon resonances together with the Ag films. As a result broadband absorption enhancement has been observed in a-Si:H solar cells deposited on these Ag coated substrates with ultrathin absorbing layers, especially in the long wavelength region. It is worth noting that fabrication of the nanodent arrays just relies on a facile anodization process, which is capable of large-scale application and especially roll-to-roll process.[30] This presents a promising route to low-cost and large-scale production of nanostructured substrates for high performance thin film solar cells. Although a similar substrate structure has been applied for μ-Si:H solar cells with a thickness of several microns,[31] the nanodent texture is well preserved even on top of the solar cells due to utilization of a much thinner a-Si:H layer, providing efficient light scattering on both sides of the a-Si:H layer.

2 Experiments and simulations

2.1 Preparation and fabrication

Fig. 1 illustrates the fabrication process of thin film devices on patterned Al substrates. Al foil with a thickness of 0.25 mm (99.999%) was first cut into small pieces (4 × 3 cm) and cleaned in acetone, ethanol and deionized water each for 15 min. Then the substrates were annealed at 450 °C for 5 h. After being etched in 1 M NaOH for 1 min to remove the native oxide layer

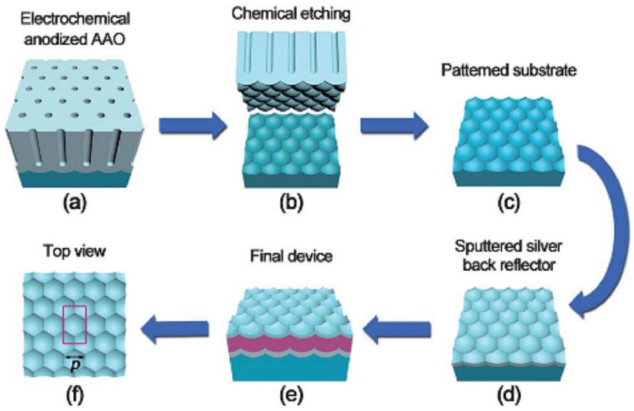

Fig. 1 Schematic procedure for fabricating a-Si:H solar cells on patterned metal substrates. (a) Electrochemically anodizing the Al foil (~4 cm × 3 cm × 250 μm). (b) Removing the porous alumina by chemical etching in a mixture of 1.8 wt% H_2CrO_4 and 6.0 wt% H_3PO_4 at 60 °C. (c) Patterned Al substrates after removal of the oxide layer. (d) Subsequently sputtering an Ag back reflector (100 nm) and BZO separation layer (30 nm). (e) Depositing n–i–p a-Si:H active layers by PECVD and sputtering the top transparent electrode (BZO, 80 nm). (f) Top view of the final device (the rectangle shows the unit cell of the periodic structure and the simulation region).

and washed by deionized water, the Al foils were anodized in a mixture of 0.3 M aqueous solution of oxalic acid and ethanol with volume ratios of 1 : 1, 1 : 2, 1 : 3, 1 : 4, 1 : 5 and 1 : 6, applying voltages of 150, 200, 250, 300, 350 and 400 V respectively for 3 h at 0 °C, a "hard anodization" condition window.[32] This can increase the anodization rate and reduce the processing time. Anodic aluminum oxide (AAO) membranes with pore intervals (D_{int}) of ~300 to 800 nm were obtained, under which (Fig. 1b) quasi-ordered hexagonal close-packed nanodent arrays were formed on the Al foils as shown in Fig. 1b and S1.† AAO membranes were etched out in a mixture of phosphoric acid (6 wt%) and chromic acid (1.8 wt%) at 60 °C for 12 h, leaving the nanodent array substrate alone (Fig. 1c). The pitch sizes (center-to-center distances) of these nanodents are denoted as p. By extending anodization duration, the degree of self-ordering of these nanodent arrays can also be improved.

Used as substrates, the patterned Al sheets were conformally coated with 100 nm Ag films, serving as back reflectors. After sputtering a 30 nm boron doped zinc oxide layer (BZO, Fig. 1d), the n–i–p a-Si:H layers were deposited by a plasma enhanced chemical vapor deposition (PECVD) method, followed by a 80 nm sputtered BZO layer as the transparent electrode (Fig. 1e). The n-type and p-type doped layers were 20 and 10 nm thick respectively, while the thickness of intrinsic a-Si:H layer varied from 70 nm to 300 nm for optimization. It is worth noting that the BZO layer between the Ag film and the n-type silicon layer acts as a buffer layer avoiding the metal diffusing into the silicon layer and provides a dielectric environment to control the plasmon resonances of the Ag film as well.

2.2 Simulations

The simulations of the optical performance were accomplished by employing Lumerical FDTD solutions with the device

construction as shown in Fig. 1e and f. A plane wave light source irradiated normally to the devices. The source was set to be polarized along the *x*-axis considering that the hexagonal arranged structure is polarization independent.[33] The unit cell of the patterned structure was set as the simulation region using anti-symmetrical boundaries in the *x*-axis, symmetrical boundaries in the *y*-axis and PML boundaries in the *z*-axis. Optical data from Palik's Handbook of Optical Constants[34] were used for Al and Ag, and BZO and n–i–p a-Si:H layers were modelled using the measured data as shown in Fig. S2.†

3 Results and discussion

3.1 Morphologies of the substrates and devices

The surface morphology of the patterned Al substrate was characterized by atomic force microscopy (AFM) and scanning electron microscopy (SEM) as shown in Fig. 2a and e and S1,† in which the hexagonally close-packed nanodent arrays can be clearly observed with an interval distance ranging from ~300 to ~800 nm as examples. Each of these nanodents possesses six tiny triangular tips at the intersections of adjacent three nanodents. A height histogram (Ht HIST, Fig. 2b) has been extracted from an AFM image, from which a maximum peak-to-valley height of about 300 nm can be observed. Radially averaged autocorrelation function (AC) is also calculated from the AFM image as shown in Fig. 2c. The oscillating behavior of the autocorrelation function confirms the long-range order of the nanodent array with a period of about 500 nm. A coherent length of about 5 microns can also be observed that is enough to cover several wavelengths of the incident light. For comparison, the SEM image of a commercial fluorine-doped tin oxide (FTO) glass (Asahi ANS14) is shown in Fig. 2d, from which no periodic feature can be observed. Afterwards the sputtered Ag back reflector and BZO separator maintain the surface morphology of the Al substrate (Fig. 2f), while a transformation from nanodents to nanodomes (Fig. 2g–i) happens after the deposition of silicon layers because of the shade effect in the subsequent coating processes. These nanodomes become larger and merge with each other when increasing the thickness of the absorbing layer.

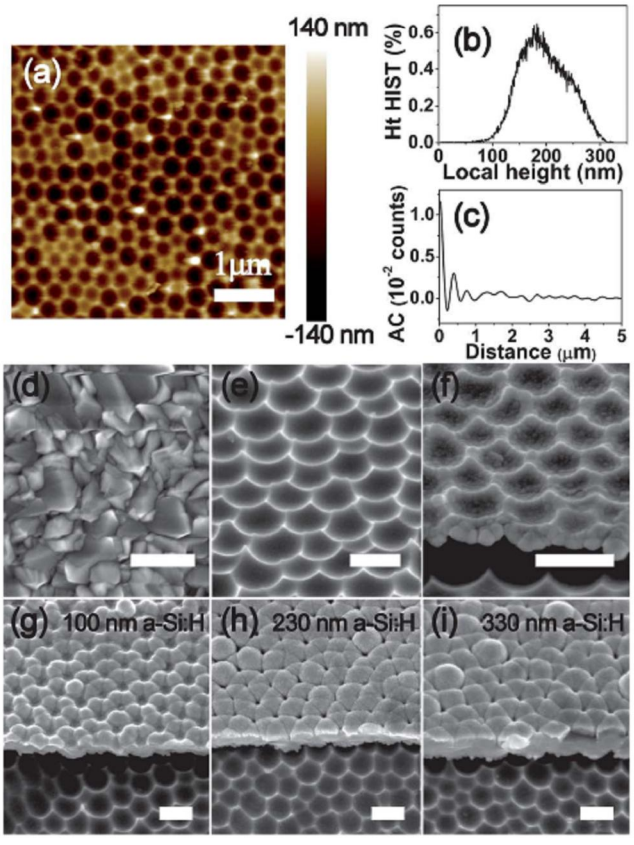

Fig. 2 AFM and SEM characterization of substrates and a-Si:H solar cells. (a) AFM image of the patterned Al substrate (p = 500 nm). (b) Height histogram of the substrate. (c) Autocorrelation function of the substrate. (d) SEM image of Asahi ANS14 glass as a reference. (e) Tilted view (~45°) of the patterned Al substrate. (f) Sputtered Ag and BZO thin films on the Al substrate (tilt angle ~45°). (g–i) Surface morphologies of the devices with different thicknesses: (g) 100 nm silicon, (h) 230 nm silicon and (i) 330 nm silicon. The scale bars in all SEM images represent 500 nm.

3.2 Measurements and simulations on optical properties

Photographs in Fig. 3a–d give an intuitional view of the light-trapping effect with the patterned substrates. Devices on patterned substrates (Fig. 3b–d) are obviously darker than that on polished planar substrates (Fig. 3a). And a thinner cell (Fig. 3b, 100 nm a-Si:H layer) shows a dark red color while a thicker cell (Fig. 3d, 330 nm a-Si:H layer) appears to be dark blue.

Reflectance measurements are carried out to confirm these observations (Fig. 3e). Compared with the device grown on the polished Al substrate, the remarkable and broadband reduction of reflectance explains the darkening in photographs. Fig. S3a† shows the absorption enhancement calculated from the

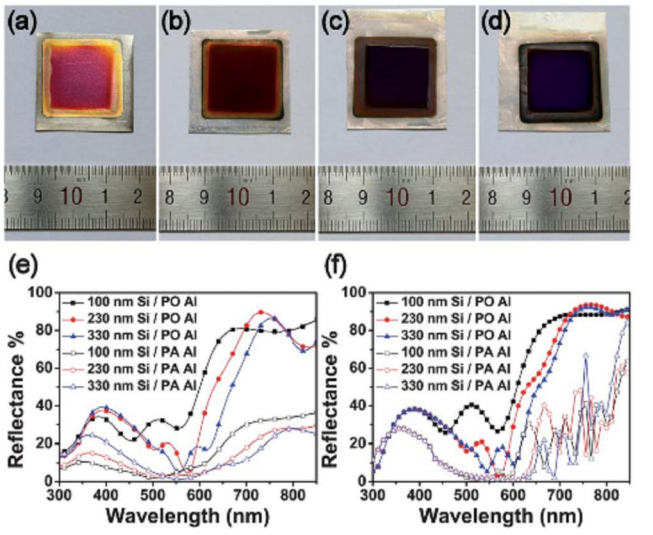

Fig. 3 (a–d) Photographs of the devices built on (a) polished Al with a 230 nm silicon layer and patterned Al with (b) 100 nm, (c) 230 nm and (d) 330 nm silicon layers. (e) Measured and (f) calculated reflectance curves of solar cells built on polished (PO) and patterned (PA, p = 500 nm) Al with different thicknesses of silicon layers.

experimental results on the Al substrate with 500 nm pitch, representing a maximum factor of 8 times. It is worth noting that these enhancement factors involve the whole devices, not only the silicon absorbing layers. Consequently, numerical simulations are carried out using the FDTD method as follows to deduce the real absorption of silicon absorbing layers (see ESI† for details).

The reflectance spectra are firstly calculated using the modelled device configuration as shown in Fig. 1e and f. Compared with the experimental results, the thickness dependence of reflectance cannot be found in short wavelength, due to the conformal surface morphology in the modelled structure. In addition, notable vibration with sharp peaks is observed in the long wavelength region on the patterned devices. This can be ascribed to the strong resonances occurring in the perfectly ordered structures in the simulation model.[2,27,31,35] In spite of these deviations, the calculated results can still reproduce the experimental trends well and thus encourage further investigation on the optical performance of the absorbing layer to understand the broadband absorption enhancement.

Fig. 4a shows the contour plot of absorption in patterned silicon layers (500 nm pitch) depending on thickness and photon energy. A broadband absorption is realized above 1.7 eV.

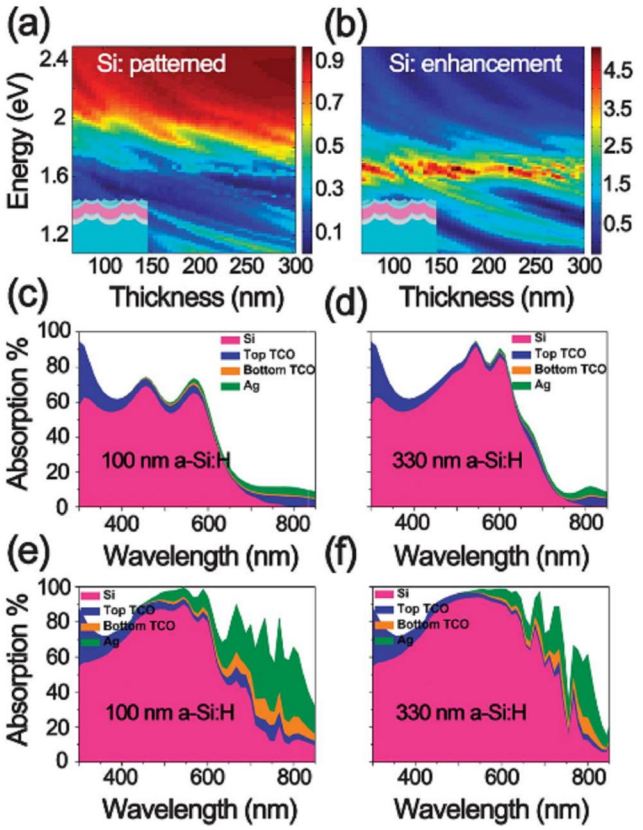

Fig. 4 Contour plot of calculated (a) absorption of a-Si:H on a patterned substrate and (b) absorption enhancement (log scale) depending on thickness and photon energy. (c–f) Plots of calculated absorption in each layer in (c and d) planar and (e and f) patterned (p = 500 nm) devices with absorbing layers of (c and e) 100 nm and (d and f) 330 nm. Insets in (a) and (b) depict the modelled structures of the corresponding devices.

For comparison, the plot of planar silicon absorption is shown in Fig. S4a,† in which obvious interference fringes and poor absorption near band edge can be observed. The enhancement factor, defined by the ratio between the absorption of silicon on patterned and planar devices on a logarithmic scale, is depicted in Fig. 4b, which presents a complementary pattern to the absorption of the planar device. This implies that the nanodent structure can significantly improve the absorption near band edge and the regions of destructive interference. The enhancement can also be identified in the absorption profiles (Fig. 4c–f and S4b and c†). Besides the enhancement in short wavelength due to the weakened interference effect, devices on patterned substrates show obviously improved absorption in long wavelengths (>600 nm) owing to the prolonged optical path length. Particularly, the enhancement factor reaches as high as 3–30 times in the long wavelength region near the band edge (>700 nm) with 100 nm, 230 nm and 330 nm silicon layers (Fig. S3b†).

The role of the thickness of a semiconductor has been studied by Saeta *et al.*, using a quasi-analytic method.[36] Greater enhancements can be obtained with thicker silicon layers, which can increase the fraction of light coupled in photonic guided modes and decrease the importance of comparatively lossy plasmon resonances. As a result shown in Fig. 4e and f, the fraction absorbed in silicon increases and the plasmon induced loss in Ag decreases as the thickness of a-Si:H increases from 100 nm to 330 nm. In addition, the spacer layer thickness is also found to be a critical factor affecting the intensity, frequency, and coupling efficiency of plasmon resonances.[23,37] However, optimized spacer layer thickness is still in suspense, especially on these complex plasmonic structures. In the case of a nanodent array substrate, the role of the spacer layer between a-Si:H and Ag back reflector will be discussed separately in another study.

Besides the scattering and gradient effective refractive index induced anti-reflection effect in the short wavelength region, two more mechanisms may account for the enhancement in the long wavelength region where the surface plasmon resonances and waveguide modes could be excited. To study the surface plasmon resonances alone, absorption of the Ag back reflector is calculated in a modelled structure with a semi-infinite silicon layer (inset in Fig. 5a), in which no photonic modes will be excited.[33] It is plotted as a 2-D contour in Fig. 5a, with reciprocal lattice constant G ($G = 2\pi/p$, where p is the interval distance in nanometer) as x axial and photon energy as y axial. Three distinct dispersive curves (marked by "S1", "S2" and "S3") can be observed, in which the plasmon resonance wavelengths undergo obvious red shifts when decreasing G (larger interval distance p). This is a typical characteristic of surface plasmon polaritons (SPPs).[38,39] Transverse momentum mismatch between the incident light and the SPP modes is compensated by the periodic patterns, resulting in the excitation of SPPs.[40] In addition, there is a prominent broad absorption band centered at ~1.3 eV (~954 nm) stretching over the full range of G values, which does not show strong dispersion like SPP modes. This feature corresponds to the localized surface plasmon resonance (LSP, marked by "L") supported by the individual tips in the Ag back reflectors.[16,41]

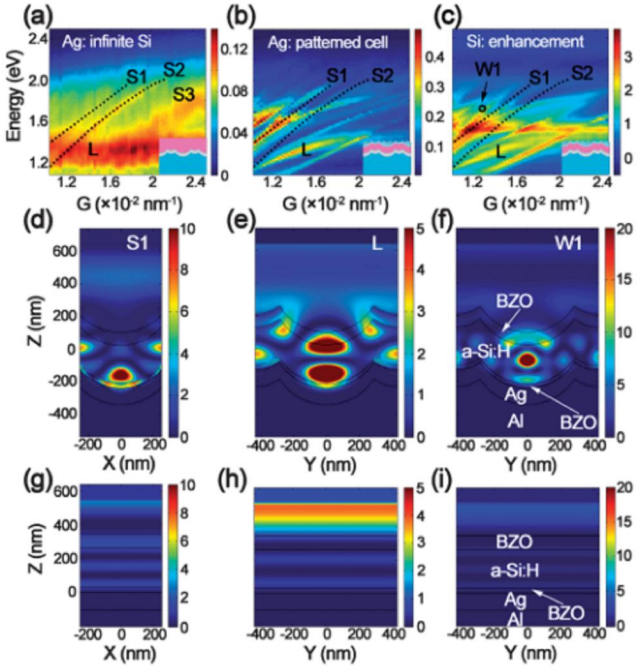

Fig. 5 Contour plot of calculated (a) absorption of an Ag back reflector with a semi-infinite silicon layer, (b) absorption of an Ag back reflector in actual configuration and (c) absorption enhancement (log scale) of a silicon layer in actual configuration. (d–i) Electric field ($|E|^2$) distributions in (d–f) patterned (p = 500 nm) and (g–i) planar devices with a 230 nm absorbing layer at a wavelength of (d and g) 799 nm, (e and h) 1011 nm and (f and i) 755 nm. Insets in (a)–(c) depict the modelled structures of the corresponding devices.

As for the actual device structure with a 230 nm silicon layer (Fig. 5b), absorption in the Ag back reflector appears to be quite different. First, the LSP resonance displays slight red shift with decreased G (larger interval distance), which could originate from the increased size of triangular pyramids at the intersections of adjacent three nanodents. The dependence of resonance frequency on dimension has been widely investigated in the research of plasmonic metal nanoparticles.[42] The reason it cannot be observed in Fig. 5a is due to the overlap of SPP modes and LSP resonance. Besides SPP modes (S1 and S2), some new dispersion features appear in Fig. 5b. These new features are attributed to waveguide modes excited within the patterned multi-layer structure and the absorption enhancement directly results from the increased field intensity within the Ag layer.[16,32] LSP and light scattering occurred on the patterned reflector contribute to the coupling of these guided modes.[43,44] Because of the coverage of the guided modes, SPP mode S3 cannot be recognized.

Absorption enhancement factors of the silicon absorbing layer are then calculated to study the real contribution of surface plasmon resonances and waveguide modes to the optical performance, as shown in Fig. 5c. The enhancement pattern shows similar features to those found in the absorption of the Ag back reflector. The influence of SPPs on the optical performance of solar cells has been discussed in many studies.[16,33,39,41] They are expected to improve absorption by confining the coupled electromagnetic energy at the metal–dielectric or metal–semiconductor interface and propagating laterally. Concealed by the waveguide modes, SPP modes S1 and S2 can hardly be observed directly in Fig. 5c. The enhancement factor reaches 28 and 3 folds at the resonance frequencies of S1 and S2. The former one is a summation of both SPP and guided modes, while the latter is a result of SPP mode alone (S2). Electric field distribution at a wavelength of 799 nm (p = 500 nm) in Fig. 5d presents the bounded energy at the surface of the Ag back reflector by SPP mode S1. Dispersions of LSP resonance and guided modes can be still observed, implying that they lead to obvious absorption enhancement in a specific wavelength region. At the tips, there exists a strong near field absorption (Fig. 5e) which confirms the LSP resonance at a wavelength of 1011 nm. In spite of the poor absorption ability of a-Si:H in this wavelength region, more effective absorption enhancement is expected to be realized by tuning LSP resonance frequency to the visible light region through changing the size,[42] shape,[45,46] plasmonic materials[42] and surrounding dielectrics[15,47] of individual triangular pyramids. The competition between Ag and semiconductors in absorbing plasmon coupled energy has been investigated by Niraj N. Lal and coworkers, showing that the absorption ratio of a-Si:H on the Ag substrate decreases for energies approaching the bandgap while the dissipation in Ag is significant.[37] So a spacer layer is recommended between a-Si:H and Ag. With a 30 nm BZO spacer layer, the results here indicate that plasmon resonances are still beneficial for silicon layer absorption. In-depth investigation on optimizing spacer thickness is highly desired for further performance enhancement. The greatest contribution to the absorption enhancement comes from the coupling of several waveguide modes. For instance, at a wavelength of 755 nm, most of the energy is confined within the silicon layer by guided mode W1 (Fig. 5f).

For comparison, electric field distributions of planar devices are also carried out in Fig. 5g–i. Without nanostructured substrate induced SPPs, LSP and waveguide modes, only interference fringes can be observed. Electric field cannot be effectively confined within the absorbing layer, and most of the incident light passes through the silicon layer and is reflected backward.

3.3 Nanodent solar cell device characterization

The overall performances of a-Si:H solar cells built on patterned Al substrates with a 500 nm interval distance are tested as shown in Fig. 6. A broadband improvement is presented in quantum efficiency (QE) measurements (Fig. 6a) compared with devices on bare glass, implying the optical absorption enhancement. The performance of cells on patterned Al substrates is also competitive as compared to that on commercial Asahi ANS14 textured FTO glass. The almost overlapped QE plots in the short wavelength region (<540 nm) indicate an excellent antireflection effect of the top surface. Enhancement in the long wavelength region originates from the SPPs and guided modes on the quasi-ordered substrate.

The I–V test under AM 1.5 irradiation (Fig. 6b) presents an open circuit voltage (V_{oc}) of 0.893 V, a short circuit current (J_{sc}) of 12.8 mA cm^{-2}, a fill factor (FF) of 0.62 and an energy conversion efficiency (η) of 7.11%, among which J_{sc} and η are improved by 31% and 27% respectively over the flat device

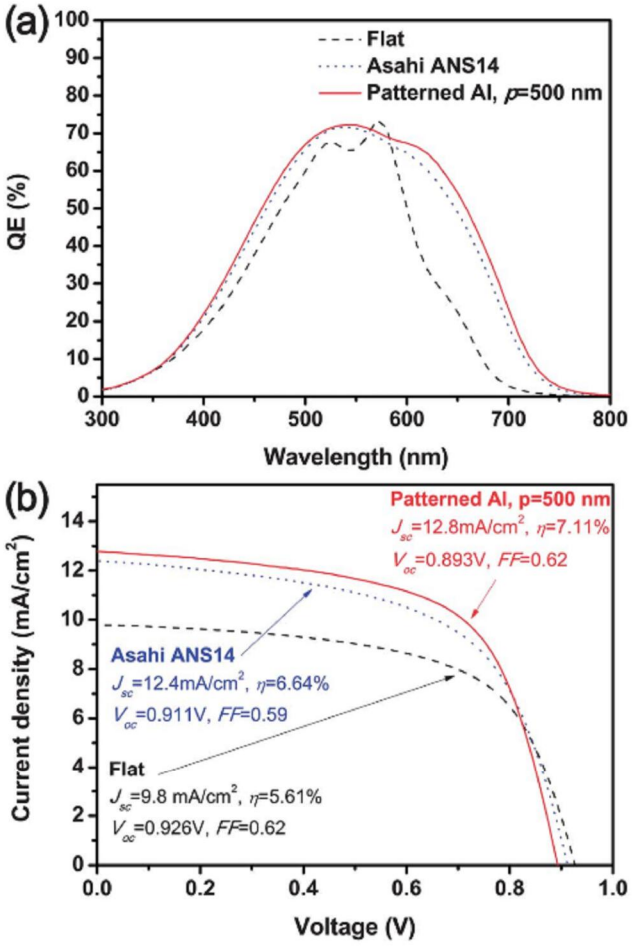

Fig. 6 (a) Quantum efficiency and (b) *I–V* curves under AM 1.5 irradiation of a-Si:H solar cells built on a patterned Al substrate ($p = 500$ nm), Asahi ANS14 FTO glass and flat glass.

($V_{oc} = 0.926$ V, $J_{sc} = 9.8$ mA cm^{-2}, FF = 0.62, $\eta = 5.61\%$), and are even better than those of cells on Asahi ANS14 glass ($V_{oc} = 0.911$ V, $J_{sc} = 12.4$ mA cm^{-2}, FF = 0.59, $\eta = 6.64\%$). To test the reliability, four samples are fabricated on each kind of substrates as shown in Fig. S5 and Table S1.† Although V_{oc} is slightly decreased owing to the texture induced defects on the patterned Al,[48] the overall performance on patterned Al is still improved remarkably, originating from the enhanced optical absorption and increased photocurrent. Compared with cells on Asahi ANS14 glass, J_{sc} on patterned Al is even higher, showing a better light trapping effect. An improved FF can also be observed, which results from the better conductivity of the metal substrate and the advantage of the U-shape geometry of patterned Al on avoiding the cracks forming in the V-shape valley.[27,49] These results match well with the optical measurements and simulation data, showing the outstanding performance of patterned Al substrates in light management of thin film solar cells.

4 Conclusions

We have demonstrated a novel approach to produce nano-textured metal substrates for constructing a-Si:H thin film solar cells. A remarkable and broadband optical absorption enhancement is realized on these nanodent array substrates. Experimental measurements and numerical calculations reveal that the enhancement comes from the efficient scattering of light in the short wavelength region and the excitation of SPP modes, LSP resonances and waveguide modes in the long wavelength region. In addition, further improvement can be carried out to reduce the anodizing time with higher growth rate by optimizing the electrolyte and process temperature. And a more economic in-suit reverse bias process can be also applied to remove the anodic oxide layer instead of wet-etching.[50] In conjunction with a roll-to-roll anodization process,[30] this work will lead to a new promising route towards large scale and low cost thin film solar cells with improved performance.

Acknowledgements

We thank Prof. Zhongyang Wang, Prof. Shanli Wang and Yunhua Wu for their helpful discussions and technical assistance. This work was financially supported by Science & Technology Commission of Shanghai Municipality (Grant no. 10DZ1210300), the 973 Program of China (Grant no. 2011CB933300), the National Natural Science Foundation of China (Grant no. 51102271, 11174308, 21001046, 51002059), the Program for New Century Excellent Talents of the University in China (Grant no. NCET-11-0179), Natural Science Foundation of Shanghai (Grant no. 11ZR1436300), Shanghai Rising-Star Program (Grant no. 11QA1406400), and Shanghai Talent Development Fund (Grant no. 2011033), General Research Fund (612111) from Hong Kong Research Grant Council and Hong Kong Innovation Technology Fund ITS/192/11.

Notes and references

1 C. R. Wronski, *IEEE Trans. Electron Devices*, 1977, **24**, 351–357.
2 V. E. Ferry, M. A. Verschuuren, H. B. T. Li, E. Verhagen, R. J. Walters, R. E. I. Schropp, H. A. Atwater and A. Polman, *Opt. Express*, 2010, **18**, A237–A245.
3 O. Kluth, B. Rech, L. Houben, S. Wieder, G. Schope, C. Beneking, H. Wagner, A. Loffl and H. W. Schock, *Thin Solid Films*, 1999, **351**, 247–253.
4 J. Muller, B. Rech, J. Springer and M. Vanecek, *Sol. Energy*, 2004, 77, 917–930.
5 P. Campbell and M. A. Green, *J. Appl. Phys.*, 1987, **62**, 243–249.
6 Z. Y. Fan, H. Razavi, J. W. Do, A. Moriwaki, O. Ergen, Y. L. Chueh, P. W. Leu, J. C. Ho, T. Takahashi, L. A. Reichertz, S. Neale, K. Yu, M. Wu, J. W. Ager and A. Javey, *Nat. Mater.*, 2009, **8**, 648–653.
7 Z. Y. Fan, R. Kapadia, P. W. Leu, X. B. Zhang, Y. L. Chueh, K. Takei, K. Yu, A. Jamshidi, A. A. Rathore, D. J. Ruebusch, M. Wu and A. Javey, *Nano Lett.*, 2010, **10**, 3823–3827.
8 R. Yu, K. L. Ching, Q. F. Lin, S. F. Leung, D. Arcrossito and Z. Y. Fan, *ACS Nano*, 2011, **5**, 9291–9298.
9 K. Q. Peng, Y. Xu, Y. Wu, Y. J. Yan, S. T. Lee and J. Zhu, *Small*, 2005, **1**, 1062–1067.

10 K. Q. Peng, X. Wang, L. Li, X. L. Wu and S. T. Lee, *J. Am. Chem. Soc.*, 2010, **132**, 6872–6873.

11 S. F. Leung, M. Yu, Q. F. Lin, K. Kwon, K. L. Ching, L. L. Gu, K. Yu and Z. Y. Fan, *Nano Lett.*, 2012, **12**, 3682–3689.

12 M. Yu, Y. Z. Long, B. Sun and Z. Y. Fan, *Nanoscale*, 2012, **4**, 2783–2796.

13 H. A. Atwater and A. Polman, *Nat. Mater.*, 2010, **9**, 205–213.

14 S. Pillai, K. R. Catchpole, T. Trupke and M. A. Green, *J. Appl. Phys.*, 2007, **101**, 093105.

15 K. R. Catchpole and A. Polman, *Opt. Express*, 2008, **16**, 21793–21800.

16 R. A. Pala, J. White, E. Barnard, J. Liu and M. L. Brongersma, *Adv. Mater.*, 2009, **21**, 3504–3509.

17 S. S. Kim, S. I. Na, J. Jo, D. Y. Kim and Y. C. Nah, *Appl. Phys. Lett.*, 2008, **93**, 073307.

18 M. D. Brown, T. Suteewong, R. S. S. Kumar, V. D'Innocenzo, A. Petrozza, M. M. Lee, U. Wiesner and H. J. Snaith, *Nano Lett.*, 2011, **11**, 438–445.

19 Y. M. Chi, H. L. Chen, Y. S. Lai, H. M. Chang, Y. C. Liao, C. C. Cheng, S. H. Chen, S. C. Tseng and K. T. Lin, *Energy Environ. Sci.*, 2013, **6**, 935–942.

20 W. B. Hou, P. Pavaskar, Z. W. Liu, J. Theiss, M. Aykol and S. B. Cronin, *Energy Environ. Sci.*, 2011, **4**, 4650–4655.

21 S. C. Warren and E. Thimsen, *Energy Environ. Sci.*, 2012, **5**, 5133–5146.

22 S.-J. Ko, H. Choi, W. Lee, T. Kim, B. R. Lee, J.-W. Jung, J.-R. Jeong, M. H. Song, J. C. Lee, H. Y. Woo and J. Y. Kim, *Energy Environ. Sci.*, 2013, **6**, 1949–1955.

23 S. Pillai, F. J. Beck, K. R. Catchpole, Z. Ouyang and M. A. Green, *J. Appl. Phys.*, 2011, **109**, 073105.

24 O. Y. Zi, S. Pillai, F. Beck, O. Kunz, S. Varlamov, K. R. Catchpole, P. Campbell and M. A. Green, *Appl. Phys. Lett.*, 2010, **96**, 261109.

25 I. K. Ding, J. Zhu, W. S. Cai, S. J. Moon, N. Cai, P. Wang, S. M. Zakeeruddin, M. Gratzel, M. L. Brongersma, Y. Cui and M. D. McGehee, *Adv. Energy Mater.*, 2011, **1**, 52–57.

26 X. Chen, B. H. Jia, J. K. Saha, B. Y. Cai, N. Stokes, Q. Qiao, Y. Q. Wang, Z. R. Shi and M. Gu, *Nano Lett.*, 2012, **12**, 2187–2192.

27 C. M. Hsu, C. Battaglia, C. Pahud, Z. C. Ruan, F. J. Haug, S. H. Fan, C. Ballif and Y. Cui, *Adv. Energy Mater.*, 2012, **2**, 628–633.

28 J. Zhu, C. M. Hsu, Z. F. Yu, S. H. Fan and Y. Cui, *Nano Lett.*, 2010, **10**, 1979–1984.

29 C. Battaglia, C. M. Hsu, K. Soderstrom, J. Escarre, F. J. Haug, M. Charriere, M. Boccard, M. Despeisse, D. T. L. Alexander, M. Cantoni, Y. Cui and C. Ballif, *ACS Nano*, 2012, **6**, 2790–2797.

30 M. H. Lee, N. Lim, D. J. Ruebusch, A. Jamshidi, R. Kapadia, R. Lee, T. J. Seok, K. Takei, K. Y. Cho, Z. Y. Fan, H. Jang, M. Wu, G. Cho and A. Javey, *Nano Lett.*, 2011, **11**, 3425–3430.

31 H. Sai, H. Fujiwara, M. Kondo and Y. Kanamori, *Appl. Phys. Lett.*, 2008, **93**, 143501.

32 W. Lee, R. Ji, U. Gosele and K. Nielsch, *Nat. Mater.*, 2006, **5**, 741–747.

33 V. E. Ferry, L. A. Sweatlock, D. Pacifici and H. A. Atwater, *Nano Lett.*, 2008, **8**, 4391–4397.

34 E. D. Palik, in *Handbook of Optical Constants of Solids*, ed. E. D. Palik, Academic Press, United States of America, 1998, vol. 1, pp. 353–357.

35 K. Soderstrom, F. J. Haug, J. Escarre, O. Cubero and C. Ballif, *Appl. Phys. Lett.*, 2010, **96**, 213508.

36 P. N. Saeta, V. E. Ferry, D. Pacifici, J. N. Munday and H. A. Atwater, *Opt. Express*, 2009, **17**, 20975–20990.

37 N. N. Lal, H. Zhou, M. Hawkeye, J. K. Sinha, P. N. Bartlett, G. A. J. Amaratunga and J. J. Baumberg, *Phys. Rev. B: Condens. Matter Mater. Phys.*, 2012, **85**, 245318.

38 N. C. Panoiu and R. M. Osgood, *Opt. Lett.*, 2007, **32**, 2825–2827.

39 W. Wang, S. M. Wu, K. Reinhardt, Y. L. Lu and S. C. Chen, *Nano Lett.*, 2010, **10**, 2012–2018.

40 W. L. Barnes, A. Dereux and T. W. Ebbesen, *Nature*, 2003, **424**, 824–830.

41 J. N. Munday and H. A. Atwater, *Nano Lett.*, 2011, **11**, 2195–2201.

42 B. J. Messinger, K. U. Vonraben, R. K. Chang and P. W. Barber, *Phys. Rev. B: Condens. Matter Mater. Phys.*, 1981, **24**, 649–657.

43 D. Derkacs, W. V. Chen, P. M. Matheu, S. H. Lim, P. K. L. Yu and E. T. Yu, *Appl. Phys. Lett.*, 2008, **93**, 091107.

44 H. R. Stuart and D. G. Hall, *Phys. Rev. Lett.*, 1998, **80**, 5663–5666.

45 B. J. Wiley, S. H. Im, Z. Y. Li, J. McLellan, A. Siekkinen and Y. N. Xia, *J. Phys. Chem. B*, 2006, **110**, 15666–15675.

46 J. J. Mock, M. Barbic, D. R. Smith, D. A. Schultz and S. Schultz, *J. Chem. Phys.*, 2002, **116**, 6755–6759.

47 F. J. Beck, A. Polman and K. R. Catchpole, *J. Appl. Phys.*, 2009, **105**, 114310.

48 H. Sakai, T. Yoshida, T. Hama and Y. Ichikawa, *Jpn. J. Appl. Phys., Part 1*, 1990, **29**, 630–635.

49 M. Python, O. Madani, D. Domine, F. Meillaud, E. Vallat-Sauvain and C. Ballif, *Sol. Energy Mater. Sol. Cells*, 2009, **93**, 1714–1720.

50 M. L. Tian, S. Y. Xu, J. G. Wang, N. Kumar, E. Wertz, Q. Li, P. M. Campbell, M. H. W. Chan and T. E. Mallouk, *Nano Lett.*, 2005, **5**, 697–703.